



OPEN

PET imaging of colon cancer CD73 expression using cysteine site-specific ^{89}Zr -labeled anti-CD73 antibody

Kyung-Ho Jung^{1,2}, Mina Kim^{1,2}, Hye Jin Jung^{1,2}, Hyun Jung Koo^{1,2}, Jung-Lim Kim^{1,2}, Hyunjong Lee¹ & Kyung-Han Lee^{1,2}✉

CD73 is a cell-surface ectoenzyme that hydrolyzes the conversion of extracellular adenosine monophosphate to adenosine, which in turn can promote resistance to immune checkpoint blockade therapy. Immune response may therefore be improved by targeting tumor CD73, and this possibility underlines the need to non-invasively assess tumor CD73 level. In this study, we developed a cysteine site-specific ^{89}Zr -labeled anti-CD73 (^{89}Zr -CD73) IgG immuno-PET technique that can image tumor CD73 expression in living bodies. Anti-CD73 IgG was reduced with tris(2-carboxyethyl)phosphine, underwent sulfohydryl moiety-specific conjugation with deferoxamine-maleimide, and was radiolabeled with ^{89}Zr . CT26 mouse colon cancer cells, CT26/CD73 cells engineered to constitutively overexpress CD73, and 4T1.2 mouse breast cancer cells underwent cell binding assays and western blotting. Balb/c nude mice bearing tumors underwent ^{89}Zr -CD73 IgG PET imaging and biodistribution studies. ^{89}Zr -CD73 IgG showed 20-fold higher binding to overexpressing CT26/CD73 cells compared to low-expressing CT26 cells, and moderate expressing 4T1.2 cells showed uptake that was $38.9 \pm 1.51\%$ of CT26/CD73 cells. Uptake was dramatically suppressed by excess unlabeled antibody. CD73 content proportionately increased in CT26 and CT26/CD73 cell mixtures was associated with linear increases in ^{89}Zr -CD73 IgG uptake. ^{89}Zr -CD73 IgG PET/CT displayed clear accumulation in CT26/CD73 tumors with greater uptake compared to CT26 tumors ($3.13 \pm 1.70\%$ ID/g vs. $1.27 \pm 0.31\%$ ID/g at 8 days; $P = 0.04$). Specificity was further supported by low CT26/CD73 tumor-to-blood ratio of ^{89}Zr -isotype-IgG compared to ^{89}Zr -CD73 IgG (0.48 ± 0.08 vs. 2.68 ± 0.52 at 4 days and 0.53 ± 0.07 vs. 4.81 ± 1.02 at 8 days; both $P < 0.001$). Immunoblotting and immunohistochemistry confirmed strong CD73 expression in CT26/CD73 tumors and low expression in CT26 tumors. 4T1.2 tumor mice also showed clear ^{89}Zr -CD73 IgG accumulation at 8 days ($3.75 \pm 0.70\%$ ID/g) with high tumor-to-blood ratio compared to ^{89}Zr -isotype-IgG (4.91 ± 1.74 vs. 1.20 ± 0.28 ; $P < 0.005$). ^{89}Zr -CD73 IgG specifically targeted CD73 on high expressing cancer cells in vitro and tumors in vivo. Thus, ^{89}Zr -CD73 IgG immuno-PET may be useful for the non-invasive monitoring of CD73 expression in tumors of living subjects.

Keywords ^{89}Zr , CD73, Antibody, Cancer, Immuno-PET

CD73 is a glycosylphosphatidylinositol-anchored transmembrane protein encoded by the *NT5E* gene that hydrolyzes the conversion of extracellular adenosine monophosphate to adenosine (ADO). CD73 is expressed on the surface of various cancer cells, including those of the breast, colorectal region, lungs, ovaries, prostate, bladder, prostate, and pancreas, where it contributes to immuno-suppression, tumor growth, metastasis, and recurrence^{1–4}. Tumor cells constantly interact with the tumor microenvironment, which includes stromal and immune cells⁵. CD73-generated extracellular ADO in the tumor microenvironment induces immuno-evasion and stimulates cancer progression by inhibiting the activities of macrophages, phagocytes, dendritic cells, natural killer cells, T-cells, and B-cells. ADO can also dampen immune responses against tumors by activating immuno-suppressive myeloid-derived cells and regulatory T-cells^{6–9}.

¹Department of Nuclear Medicine, Samsung Medical Center, 81 Irwon-ro, Gangnam-gu, Seoul, Korea. ²Samsung Advanced Institute for Health Sciences and Technology, Sungkyunkwan University School of Medicine, Seoul, Korea. ✉email: khleenm@naver.com

Immune checkpoint therapy is revolutionizing the outcomes for patients with various types of cancers¹⁰; for example, blockade of the immune checkpoint targets PD-L1 and CTLA4 has shown remarkable antitumor effects^{11,12}. However, despite the unprecedented clinical impact of these therapies, significant limitations still must be overcome; these include varying response rates, a benefit to only a small portion of patients, and the frequent occurrence of resistance. As such, there is a need to unravel additional immune factors that influence responses to immune checkpoint therapy and to develop newer approaches to overcome the current challenges. In this regard, CD73 is highly expressed in most cancer types and is an attractive newer target to enhance the efficacy of immune checkpoint blockade^{13–15}.

Molecular imaging methods that non-invasively assess tumor CD73 expression in vivo can facilitate the preclinical and clinical development of novel CD73 blockade therapies. These techniques could overcome the limitations of invasive tissue biopsy that is subject to sampling errors inherent to the inter-patient and intra-patient heterogeneity of CD73 expression, even within the same tumor. Imaging can facilitate accurate assessment of CD73 expression in the whole tumor without causing pain to the patient to help predict therapeutic response and inform treatment decisions¹⁶. Furthermore, non-invasive imaging can be repeated to monitor changes in target antigen levels following chemotherapy¹⁷.

A recent study visualized the tumor uptake of anti-CD73 antibody that was radiolabeled with ¹¹¹In for single-photon emission computed tomography imaging¹⁸. However, positron emission tomography (PET) is required for sensitive and quantitative assessment of radiotracer distribution with superior image contrast. Indeed, immuno-PET has emerged as a useful tool to facilitate the development of novel antibody therapeutics by providing pharmacokinetic information and quantifying the tumor antigen level relevant for treatment decision-making¹⁹.

In this study, we thus developed a new immuno-PET technique based on an anti-CD73 antibody site-specifically labeled with ⁸⁹Zr that allows for specific and high-contrast imaging of tumor CD73.

Materials and methods

Cell culture and reagents

CT26 mouse colon cancer cells and 4T1.2 mouse breast cancer cells (derived from the 4T1 cell line) purchased from the American Type Culture Collection (Manassas, VA, USA) were maintained in 5% CO₂ at 37 °C in RPMI 1640 medium (Lonza, Basel, Switzerland) supplemented with 10% fetal bovine serum (FBS) (Serena, Germany), 2 mM of L-glutamine, and 100 U/mL of penicillin–streptomycin (Gibco Laboratories, Gaithersburg, MD, USA).

Rabbit antibody against NT5E/CD73 was sourced from Cell Signaling Technology (Danvers, MA, USA), while mouse antibody against β-actin and horseradish peroxidase-conjugated secondary anti-rabbit and anti-mouse antibodies were purchased from Santa Cruz Biotechnology (Dallas, TX, USA).

Preparation of CT26 cells stably overexpressing CD73

We used a CD73 (NM_011851) mouse tagged ORF clone lentiviral particle from Origene (Rockville, MD, USA). The lentiviral particle was constructed with the pLenti-C-mGFP-P2A-Puro vector that contains the *mGFP* gene and puromycin-resistance gene as selection markers. CT26 cancer cells stably overexpressing mouse CD73 (CT26/CD73 cells) were prepared by first infecting cells with the lentiviral particles, then selecting cells 72 h later under 10 µg/mL of puromycin (Thermo Fisher Scientific, Waltham, MA, USA). Single-cell clones overexpressing CD73 were picked up, amplified in media containing puromycin, and stored in liquid nitrogen as stocks. The cell clone with the greatest specific binding of the CD73 antibody probe was used for experiments.

Deferoxamine conjugation and site-specific ⁸⁹Zr labeling of anti-CD73 antibody

Rat IgG2a against mouse CD73 (clone TY/23; BioXcell, West Lebanon, NH) and isotype IgG2a (clone 2A3; BioXcell) were site-specifically conjugated with deferoxamine-maleimide on sulphydryl residues as previously described²⁰. Briefly, 2 mg of antibody was incubated with 100 mM of tris(2-carboxyethyl) phosphine (TCEP) (Sigma-Aldrich, St. Louis, MO) for 20 min at room temperature (RT) in a 1:100 molar ratio. Sulphydryl residues of IgG diluted in 0.1 M of sodium phosphate containing 150 mM of NaCl and 1 mM of EDTA were conjugated for 60 min at RT with 56.4 µL of 2 mM N-(3,11,14,22,25,33-hexaoxo-4,10,15,21,26,32-hexaaza-10,21,32-trihydroxytetracontane) maleimide (deferoxamine-maleimide; Macrocyclics, Plano, TX). The molar ratio of DFO-maleimide to antibody was 60:1. ⁸⁹Zr-oxalate (50 µL; Korea Atomic Energy Research Institute, Daejeon, South Korea) was neutralized with 25 µL of 2 M Na₂CO₃ and mixed with deferoxamine-conjugated IgG in 75 µL of 0.5 M HEPES buffer (pH, 7.5). Following 60 min of incubation at RT with tapping every 15 min, the reaction mixture was eluted through a PD-10 column with 0.25 M of sodium acetate containing 0.5% gentisic acid. Fractions of 0.5 mL were collected and counted for radioactivity on a high-energy γ-counter, and the peak activity fraction was used.

Sodium dodecyl sulfate (SDS)-polyacrylamide gel electrophoresis (PAGE) and autoradiography

For non-reducing SDS-PAGE, 2 µg of intact, TCEP-reduced, and DFO-conjugated IgG was diluted with water and 5x non-reducing sample buffer without dithiothreitol. Samples were boiled at 95 °C for 10 min, then separated on an 8% SDS polyacrylamide gel, which was subsequently stained with 0.5% Coomassie blue.

Autoradiography was also performed for ⁸⁹Zr-CD73 IgG and ⁸⁹Zr-isotype IgG, which were separated by 8% native PAGE with sample buffer without SDS or dithiothreitol.

Radiochemical stability assessment

⁸⁹Zr-CD73 IgG and ⁸⁹Zr-isotype IgG were tested for radiochemical purity and stability by radio-instant thin-layer chromatography (radio-iTLC). The radiotracers were mixed in equal volumes of PBS or FBS, finally resulting in 50% phosphate-buffered saline (PBS) and 50% FBS, respectively. The mixture was then incubated at 37 °C

for 0, 4, or 7 days. Radio-iTLC was then performed using 50 mM EDTA (pH, 5.5) as eluent on iTLC-SG glass microfiber chromatography paper impregnated with silica gel (Agilent Technologies, Santa Clara, CA). Under this condition, intact radiolabeled antibody remains at baseline while free $^{89}\text{Zr}^{4+}$ ions and [^{89}Zr]-EDTA migrate at the solvent front.

Cell-binding assays and Lindmo assays

CT26 and CT26/CD73 cells were incubated with 74 kBq of ^{89}Zr -CD73 IgG for 60 min at 37 °C in RPMI 1640 medium. Cells were then washed twice with cold PBS (pH, 7.4), lysed with 0.5 mL of 0.1 N of NaOH, and measured for radioactivity on a high-energy γ -counter. Binding specificity was evaluated in the presence of 500 nM of unlabeled anti-CD73 IgG. In addition, low expressing CT26 cells were mixed with overexpressing CT26/CD73 cells at ratios between 20 and 100% for a total of 2×10^7 cells, and immunoreactive assay was evaluated.

For Lindmo binding assays, five serial dilutions of CT26/CD73 cells (0.2–3.2 $\times 10^6$) in culture medium containing 1% bovine serum albumin were incubated with anti-CD73 IgG (final concentration of 50 ng/mL) for 45 min at RT. The cells were centrifuged and washed twice with cold PBS, and cell-bound radioactivity was counted with a high-energy γ -counter. Non-specific binding was measured in each cell dilution in the presence of 5 $\mu\text{g}/\text{mL}$ of unlabeled anti-CD73 IgG. The immunoreactivity of radiolabeled antibodies was estimated as previously described²¹. Briefly, a conventional plot was drawn of specific and non-specific binding over total applied radioactivity, as a function of increasing cell concentration. A double inverse plot was then drawn using the same data as total applied radioactivity over specific binding, as a function of the inverse cell concentration. The immunoreactive fraction was determined through linear extrapolation to the ordinate.

Western blotting of cultured cells and tumor tissue proteins

For immunoblotting, cultured cells and homogenized tumor tissues were washed with cold PBS and lysed at –20 °C for 20 min in 200 μL of PRO-PREP™ Protein Extraction Solution (iNtRON Biotechnology, Inc., Seongnam, Korea) containing protease inhibitor cocktail (P2714; Sigma-Aldrich, St. Louis, MO, USA) and phosphatase inhibitor cocktail (78420; Thermo Fisher Scientific, Waltham, MA, USA). After centrifugation at 14,000 rpm and 4 °C for 10 min, supernatants were transferred to new tubes and measured for protein concentration by Bradford assays. Protein samples amounting to 20–25 μg were then boiled for 5 min, separated by 10% SDS-PAGE, and transferred to a polyvinylidene difluoride membrane. After incubation with a rabbit monoclonal antibody against CD73 (13160s; 1:1000 dilution) overnight at 4 °C, the membranes were washed three times with TBST buffer and incubated with horseradish peroxidase-conjugated secondary anti-rabbit IgG antibodies (7074S; 1:2000) at RT for 2 h. The membranes were incubated for 2 min with 0.8 mL of enhanced chemiluminescence substrate (#32132; Thermo Fisher Scientific, Waltham, MA, USA) that was pre-mixed with components A and B in a 20:1 ratio. The luminescent signal was detected, and immunoreactive protein band intensities were quantified using Quantity One® software (Bio-Rad Laboratories, Hercules, CA, USA). After visualizing CD73 protein bands, the membrane was stripped and re-incubated with an antibody against β -actin (sc47778).

Immunohistochemistry of tumor tissues for CD37 protein

For immunohistochemistry of CD73 protein, frozen sections (6 μm thickness) of CT26 or CT26/CD73 tumor tissue incubated with a rabbit monoclonal antibody against CD73 (13160s, Cell Signaling Technology, MA; 1:100 dilution in Dako diluent solution, S3022, Dako, CA) or rat Isotype IgG2a (10 mg/ml conc.: BE0089, BioXcell, 1:2000 dilution in Dako diluent solution) overnight at 4 °C. An EnVision™ Detection system kit applied using HRP labeled polymer anti-rabbit IgG for CD73 antibody (K4003; Dako) and HRP labeled polymer anti-rat IgG for isotype IgG2a antibody (ab2 #214882; Abcam). Finally, slides were counterstained with Dako Mayer's hematoxylin (S3309, CA) and mounted with coverslips.

In vivo PET imaging and biodistribution studies in tumor models

All animal experiments were conducted in accordance with the National Institute of Health Guide for the Care and Use of Laboratory Animals and were approved by the Institute ethics committee of Samsung Medical Center. This study was carried out in compliance with the ARRIVE guidelines. Tumor models were prepared in Balb/c nude mice by subcutaneous injection of 5×10^6 CT26 cells, CT26/CD73 cells, or 4T1.2 cells into the right shoulder. Experiments were performed when the tumor diameter reached 0.5 cm at approximately 10 days after cell inoculation. CT26/CD73 and 4T1.2 tumor-bearing mice were randomly allocated into ^{89}Zr -CD73 IgG and ^{89}Zr -isotype IgG groups. At 4 days or 8 days after intravenous injection with 4.8 MBq of ^{89}Zr -CD73 IgG or ^{89}Zr -isotype IgG, isoflurane-anesthetized tumor-bearing mice underwent PET/CT imaging on an Inveon scanner (Siemens Medical Solutions, Erlangen, Germany). PET-based tumor uptake was measured on non-attenuation corrected coronal images. Tissue radioactivity was measured as %ID/g by placing regions-of-interest on the blood pool of major vessels, the lungs, the liver, muscle, and the tumor. Tumor margins were automatically delineated using a 50% threshold of maximal activity, and images were verified for inclusion of the entire tumor volume while excluding any normal tissue.

Biodistribution studies were performed in tumor-bearing mice after the final PET/CT imaging. The mice were sacrificed by cervical dislocation, and major organs and tumors were extracted, weighed, and measured for radioactivity on a high-energy γ -counter. The final results were expressed in injected dose per gram of tissue (%ID/g).

Statistical analysis

Data are presented as mean \pm standard deviation values unless otherwise specified. Differences between groups were analyzed by two-tailed unpaired Student's *t* tests for two groups and analysis of variance with Tukey's post-hoc test for three or more groups. $P < 0.05$ was considered significant.

Results

DFO-conjugation and site-specific ^{89}Zr labeling of CD73 IgG and isotype control IgG

Site-specific conjugation of deferoxamine-maleimide on sulphydryl residues of anti-CD73 IgG was achieved in a straightforward and reproducible manner. To accomplish this, the antibody was first reduced by a reaction with TCEP, followed by conjugation with deferoxamine-maleimide. SDS-PAGE demonstrated that TCEP completely reduced target disulfide bonds of the antibody and produced an antibody fragment that was half the size of the intact antibody. This reduced state was maintained after DFO-conjugation (Fig. 1A). PAGE analysis of the first peak fraction (#6 and #7) of the PD-10 column elute displayed a clear radioactive band at the expected 150-kD region (Fig. 1B).

^{89}Zr radiolabeling of DFO-conjugated anti-CD73 IgG was reproducible with an average efficiency of 75.3% ($n = 5$; Fig. 1C). Radiochemical purity was $> 99\%$, and the specific activity was 0.8 mCi/mg. Radiochemical stability as assessed by iTLC analysis showed that the radiolabel was $> 90\%$ intact after 96 h of incubation in 50% FBS as well as in 50% PBS (Fig. 1D).

Site-specific conjugation of deferoxamine-maleimide on sulphydryl residues of isotype control IgG and ^{89}Zr radiolabeling was also achieved in a straightforward fashion. The results of non-reducing PAGE analysis of TCEP-conjugated, DFO-conjugated, and amicon-filtered isotype IgG, and column chromatography, autoradiography, and iTLC analysis of in vitro stability of ^{89}Zr -isotype IgG are shown in Supplementary Fig. 1.

^{89}Zr -CD73 IgG binding to low and high CD73-expressing cancer cells

Western blotting showed that, whereas parental CT26 cells had low levels of CD73 expression, stably overexpressing CT26/CD73 cells displayed 9.7 ± 0.1 -fold of CD73 protein expression (Fig. 2A). In addition, cell binding assays demonstrated that CT26/CD73 cells had high ^{89}Zr -CD73 IgG binding, reaching 20-fold of binding to CT26

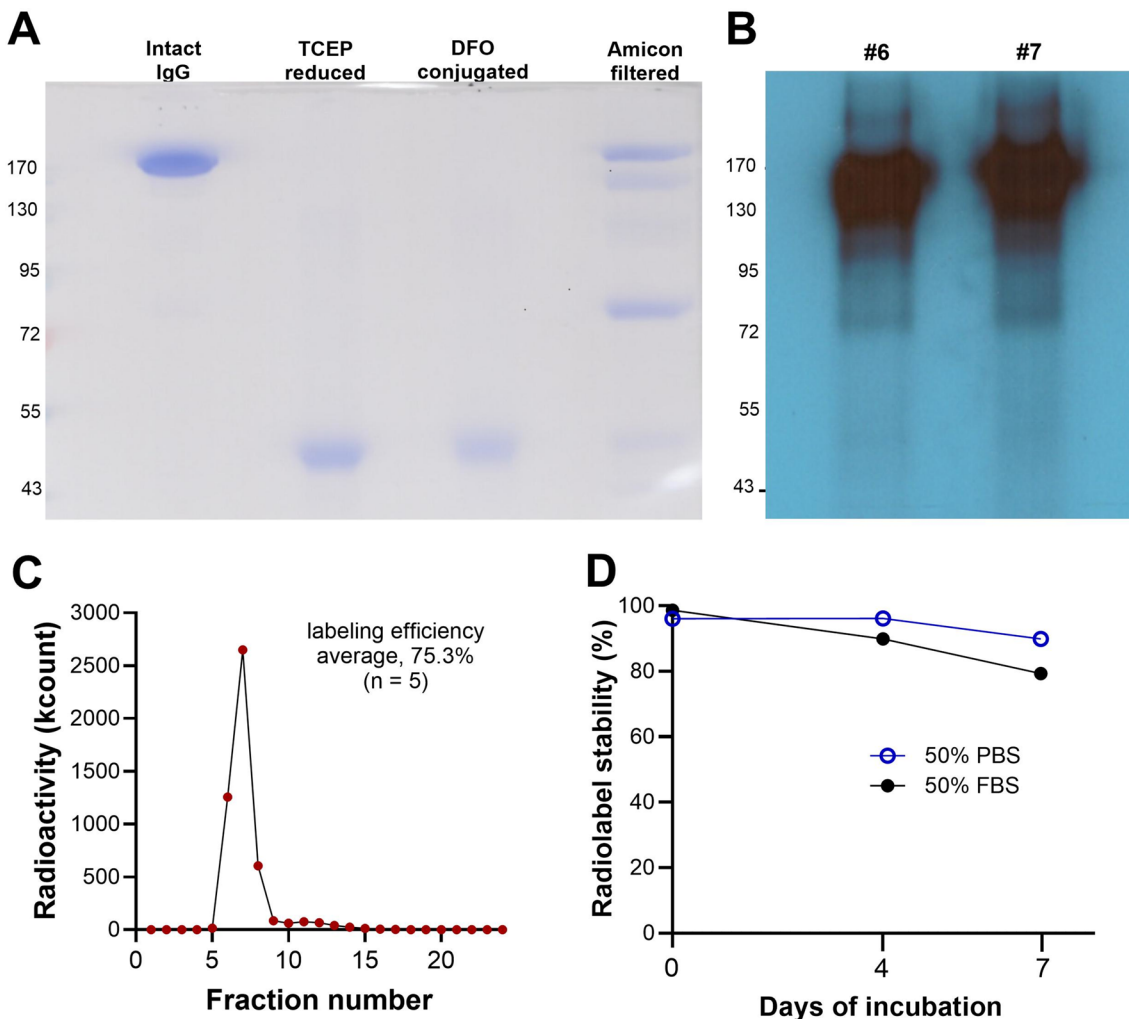


Figure 1. Cysteine-site specific ^{89}Zr labeling of anti-CD73 IgG. (A) Non-reduced SDS-PAGE of unmodified, TCEP-reduced, and DFO-conjugated anti-CD73 IgG. The Amicon filtered lane refers to DFO-conjugated antibody following Amicon filtration to remove unconjugated reagents. (B) Autoradiography of peak fractions of ^{89}Zr -CD73 IgG by native PAGE (right). (C) Radioactivity profile of PD-10 column-eluted fractions. (D) In vitro stability of ^{89}Zr -CD73 IgG assessed by radio-iTLC.

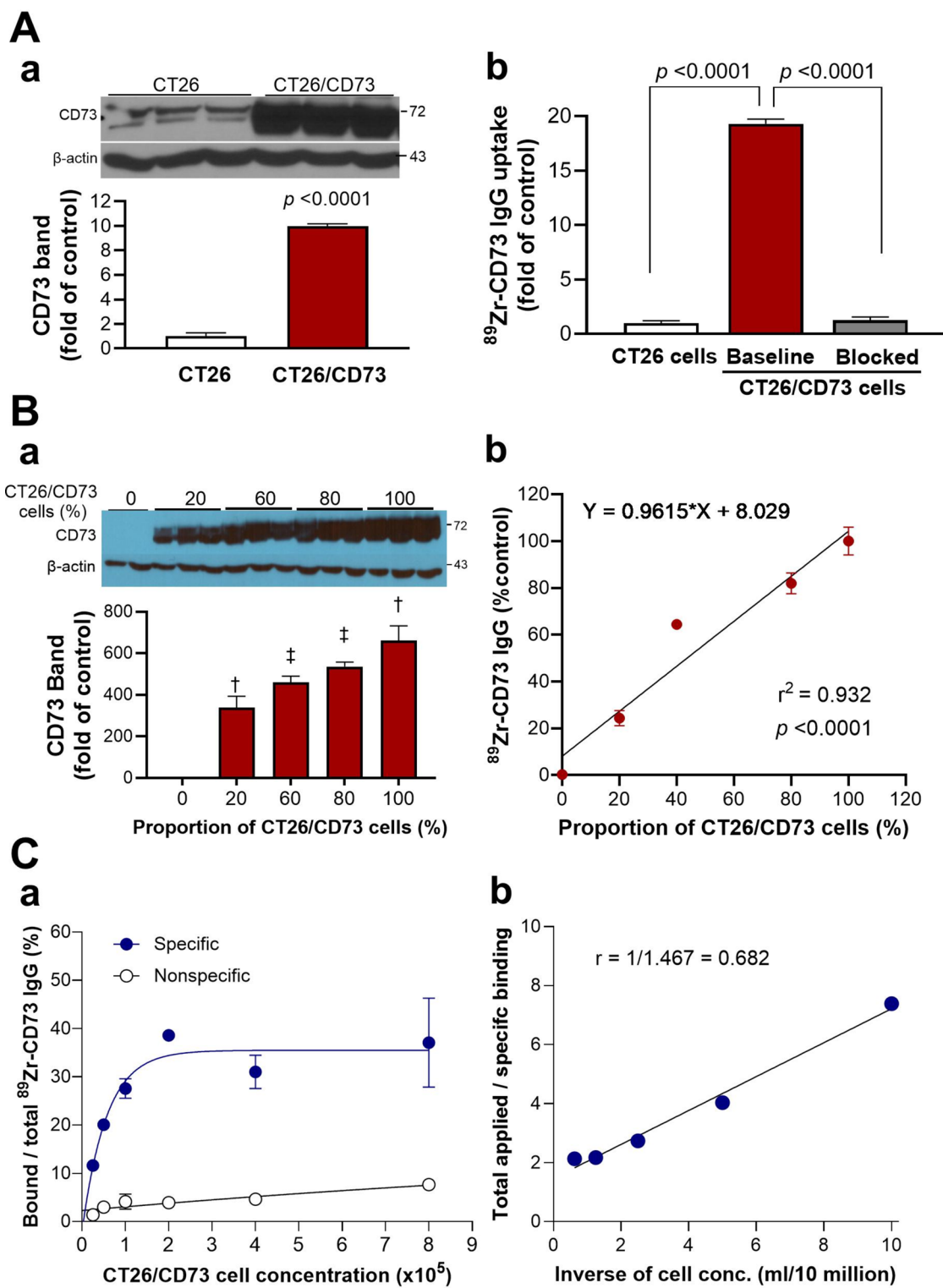


Figure 2. CD73 expression and ^{89}Zr -CD73 IgG binding in colon cancer cells. (A) (a) Immunoblotting of CD73 in low-expressing parental CT26 and high-expressing CT26/CD73 cancer cells. (b) ^{89}Zr -CD73 IgG binding in CT26, CT26/CD73 cells, and in CT26/CD73 cells blocked with excess unlabeled anti-CD73 antibody. (B) The CD73 protein amount (a) and ^{89}Zr -CD73 IgG uptake level, (b) are increased proportionally to the CT26/CD73 cell content in a mixture of CT26/CD73 and CT26 cells. (C) Representative Lindmo binding assay. A conventional plot of specific and non-specific binding over total applied radioactivity, as a function of increasing cell concentration, is shown (a). A double inverse plot was drawn using the same data as those describing total applied radioactivity over specific binding, as a function of the inverse cell concentration (b). The immunoreactive fraction was determined through linear extrapolation to the ordinate. All data are the mean \pm standard deviation values obtained from a single experiment ($n=3$ per group).

cells. This high binding was completely abolished to $6.5\% \pm 1.7\%$ of the unblocked level in the presence of 500 nM of cold anti-CD73 IgG (Fig. 2A), which was a 56.6-fold concentration compared to the 8.8 nM of radiolabeled antibody. This indicated excellent target specificity of binding.

When CT26 cells and CT26/CD73 cells were mixed in graded proportions, immunoblots showed that the CD73 protein amount was increased proportionately to the CT26/CD73 cell content (Fig. 2B). This was faithfully reflected by CT26/CD73 cell content-dependent linear increases in ^{89}Zr -CD73 IgG uptake (Fig. 2B). This shows that the magnitude of cellular ^{89}Zr -CD73 IgG binding in vitro correlates to target CD73 protein level. Lindmo assays of ^{89}Zr -CD73 IgG showed an average immunoreactive fraction of $55.4 \pm 18.1\%$ ($n = 2$; Fig. 2C).

An additional model utilized 4T1.2 mouse breast cancer cells that express physiological levels of CD73. Western blots confirmed that 4T1.2 cells express moderate amounts of CD73 that was $51.8 \pm 13.9\%$ of CT26/CD73 cells ($P < 0.005$; Fig. 3A). Binding experiments showed that 4T1.2 cells took up ^{89}Zr -CD73 IgG in magnitudes $38.9 \pm 1.51\%$ of CT26/CD73 cells. This uptake was near completely blocked to $12.2 \pm 1.4\%$ of the unblocked level by 500 nM of unlabeled CD73 IgG (Fig. 3B).

In vivo target specificity of CT26/CD73 tumor ^{89}Zr -CD73 IgG uptake at 4 days post-injection

At 4 days post-injection, ^{89}Zr -CD73 IgG PET images showed clear visualization of CT26/CD73 tumors that had high contrast uptake compared to CT26 tumors with low relative uptake. In a separate group of CT26/CD73 tumor mice injected with ^{89}Zr -labeled IgG2a-isotype antibody, PET images showed diffuse non-specific activity in the blood pool and major organs and tumor (Fig. 4A).

Biodistribution data reiterated these findings by confirming greater ^{89}Zr -CD73 IgG uptake in CT26/CD73 tumors ($4.16 \pm 0.8\%$ ID/g) compared to CT26 tumors ($1.52 \pm 0.4\%$ ID/g; $P < 0.001$; Fig. 4B). Furthermore, CT26/CD73 tumor-to-blood ratio was significantly higher for ^{89}Zr -CD73 IgG compared to ^{89}Zr -isotype IgG (2.68 ± 0.52 vs. 0.48 ± 0.08 ; $P < 0.0001$; Fig. 4C). These findings support the target specificity of tumor ^{89}Zr -CD73 IgG uptake in living mice. At this time point, however, ^{89}Zr -CD73 IgG activities in the kidneys and liver in CT26/CD73 tumor mice remained greater than tumor uptake, which could be an obstacle for imaging intraabdominal tumors. Therefore, we repeated PET/CT imaging and biodistribution studies at a more delayed time of 8 days.

^{89}Zr -CD73 IgG PET and biodistribution of in CT26 and CT26/CD73 tumor mice at day 8

PET/CT imaging at 8 days after ^{89}Zr -CD73 IgG injection displayed clear visualization of high uptake in CT26/CD73 tumors, whereas CT26 tumors showed low uptake. Importantly, activity in the liver, spleen, and kidneys at this delayed time point was relatively low (Fig. 5A). Eight-day biodistribution data confirmed high ^{89}Zr -CD73 IgG accumulation in CT26/CD73 tumors that reached $3.13 \pm 1.70\%$ ID/g. This amounted to 2.5-fold of the uptake for low-expressing CT26 tumors ($1.27 \pm 0.31\%$ ID/g; $P < 0.05$; Fig. 5B). Uptake in the liver, spleen, and kidneys at this time point was lower than tumor uptake level.

PET images and biodistribution results of ^{89}Zr -isotype IgG at day 8 showed significant tumor activity ($4.34 \pm 0.83\%$ ID/g) but substantially higher blood activity ($8.15 \pm 1.08\%$ ID/g). Consequently, the tumor-to-blood ratio remained low ($0.53 \pm 0.07\%$ ID/g) compared to the ninefold higher ratio for ^{89}Zr -CD73 IgG ($4.81 \pm 1.02\%$ ID/g; Fig. 5C).

CD73 expression in CT26 and CT26/CD73 tumor tissues

Immunoblotting of protein from tumor tissues at day 8 displayed strong CD73 bands for CT26/CD73 tumor tissues compared to weak bands for CT26 tumors (Fig. 6A). Immunohistochemistry also showed strong CD73 staining CT26/CD73 tumor tissues compared to weak staining for CT26 tumors (Fig. 6B). These findings were considered consistent with the PET/CT and biodistribution results. Immunohistochemistry using rat Isotype

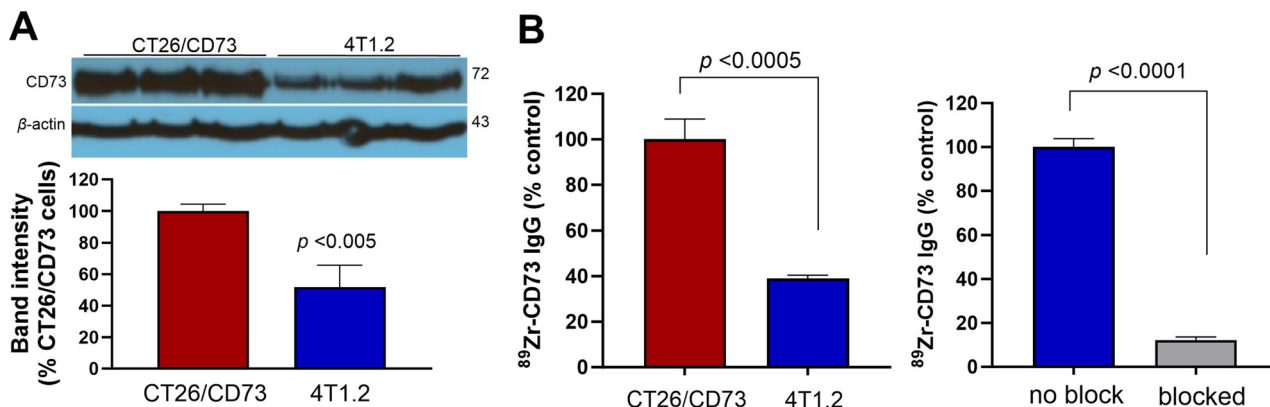


Figure 3. CD73 expression and ^{89}Zr -CD73 IgG binding in 4T1.2 breast cancer cells. (A) Immunoblotting and quantified band intensities of CD73 protein in 4T1.2 cells compared to overexpressing CT26/CD73 cells. (B) ^{89}Zr -CD73 IgG binding in 4T1.2 cells compared to equal number of CT26/CD73 cells, and effect of blocking with excess unlabeled anti-CD73 antibody. All data are the mean \pm standard deviation values obtained from a single experiment ($n = 3$ per group).

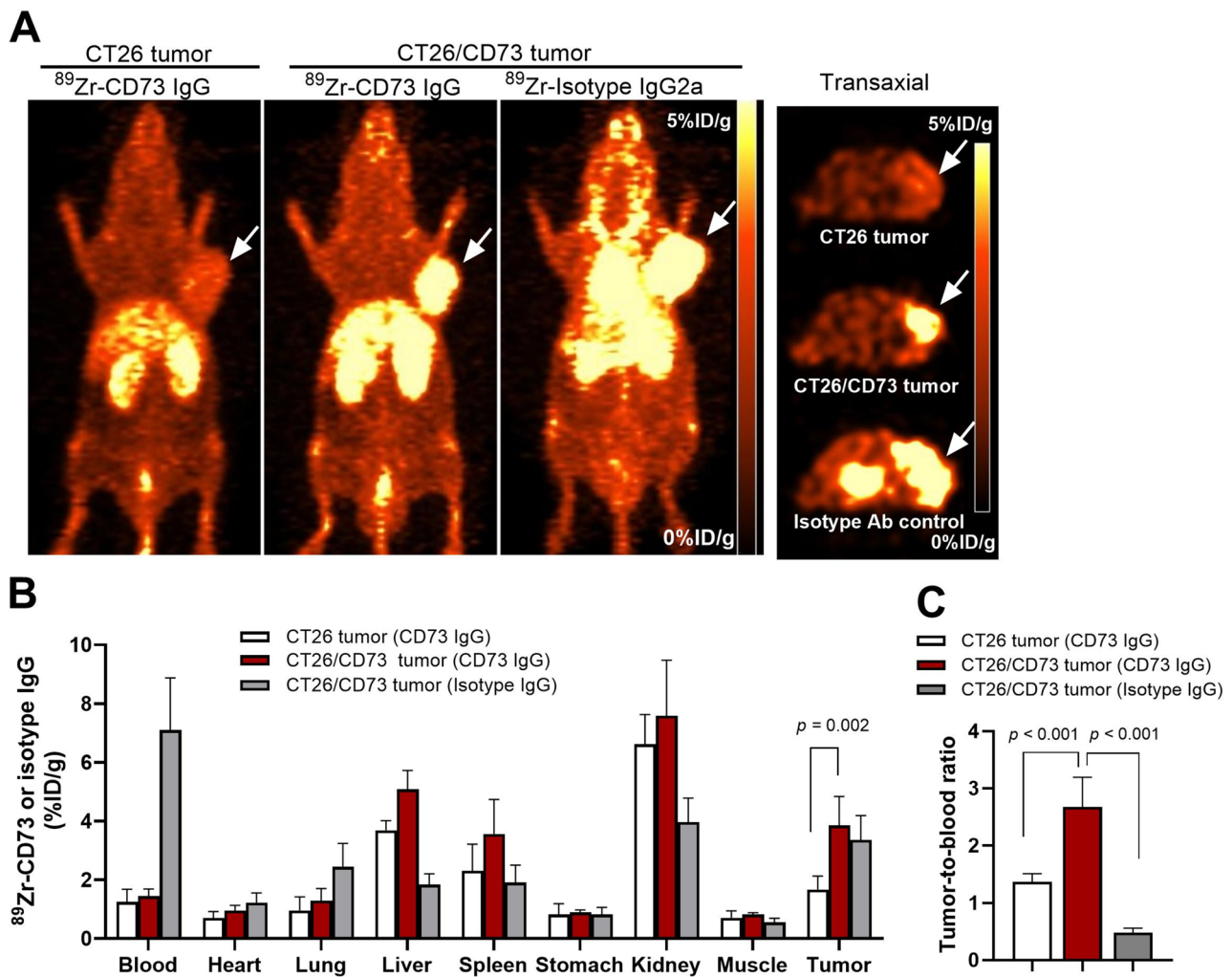


Figure 4. ^{89}Zr -CD73 IgG PET/CT and biodistribution at 4 days in CT26 and CT26/CD73 tumor mice. (A) Coronal and transaxial tomographic PET images at 4 days post-injection showing high ^{89}Zr -CD73 IgG uptake in CT26/CD73 tumors (arrow). CD73-specific uptake was verified by low ^{89}Zr -CD73 IgG accumulation in CT26 tumors. Target specificity was further supported by low CT26/CD73 tumor-contrast in a separate control group injected with ^{89}Zr -isotype IgG. (B) Biodistribution data reiterated these findings by confirming greater ^{89}Zr -CD73 IgG uptake in CT26/CD73 tumors compared to CT26 tumors. (C) Furthermore, the CT26/CD73 tumor-to-blood ratio was significantly higher for ^{89}Zr -CD73 IgG compared to ^{89}Zr -isotype IgG. Data are presented as the mean \pm standard deviation values obtained from a single experiment ($n=5$ per group).

IgG2a antibody as negative control confirmed the absence of specific signals in both CT26 and CT26/CD73 tumor microsections (Suppl Fig. 2).

^{89}Zr -CD73 IgG PET and biodistribution of in 4T1.2 tumor mice at day 8

In 4T1.2 tumor-bearing mice, PET/CT imaging at 8 days after ^{89}Zr -CD73 IgG injection showed clear tumor visualization (Fig. 7A) and biodistribution results confirmed that tumor uptake reached $3.75 \pm 0.70\%$ ID/g while blood activity was only $0.83 \pm 0.24\%$ ID/g (Fig. 7B). Although PET images with control ^{89}Zr Isotype IgG also showed visualization of 4T1.2 tumors ($5.68 \pm 1.49\%$ ID/g), this was accompanied by high blood activity ($4.80 \pm 1.07\%$ ID/g). As a result, the tumor-to-blood pool ratio for ^{89}Zr -Isotype IgG was low at 1.20 ± 0.28 , compared to a high ratio of 4.91 ± 1.74 by ^{89}Zr -CD73 IgG (Fig. 7C).

Together, the biodistribution results in the two tumor models support the notion that the tumor activity of ^{89}Zr -isotype IgG was likely contributed by nonspecific intra-tumoral blood pool activity, whereas tumor accumulation of ^{89}Zr -CD73 IgG was the result of specific target binding.

Discussion

CD73 is highly expressed in various cancer types and regulates extracellular ADO concentration by its production through the dephosphorylation of adenosine monophosphate. CD73 suppresses tumor immune responses by inhibiting antitumor T-cell activity and enhancing the immune inhibitory function of cancer-associated fibroblasts and myeloid cells. Therefore, blockade of CD73 function is a promising strategy for combination treatment

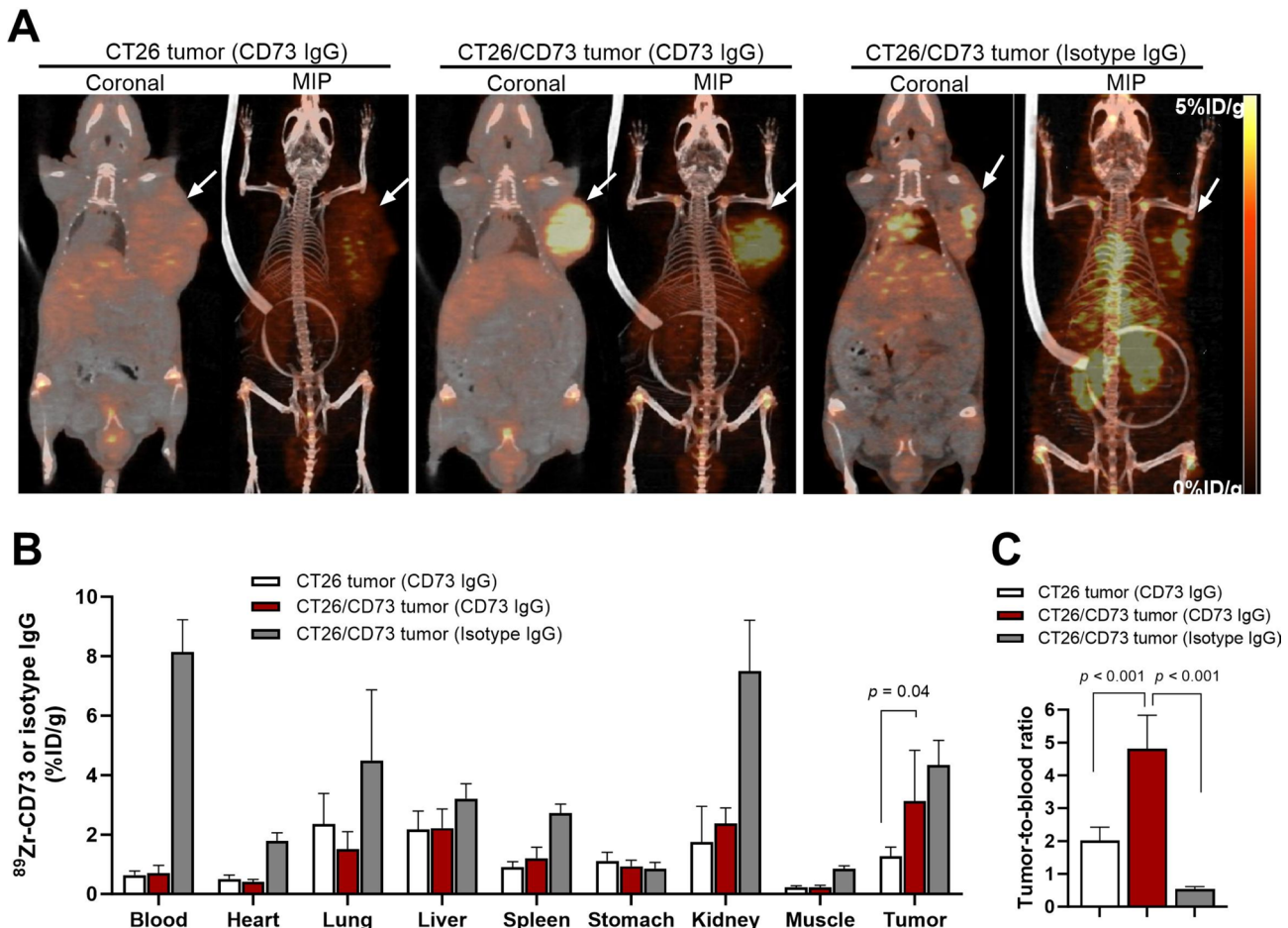


Figure 5. ^{89}Zr -CD73 IgG PET/CT and biodistribution at 8 days in CT26 and CT26/CD73 tumor mice. (A) Coronal tomographic and maximum intensity-projection (MIP) ^{89}Zr -CD73 IgG PET/CT in CT26 (left) or CT26/CD73 tumor-bearing mice (middle), and ^{89}Zr -isotype IgG PET/CT in CT26/CD73 tumor mice (right). (B) Biodistribution data of mice as above at 8 days post-injection. (C) Again, the CT26/CD73 tumor-to-blood ratio was significantly higher for ^{89}Zr -CD73 IgG compared to ^{89}Zr -isotype IgG. Data are the mean \pm standard error of obtained from two independent experiments ($n = 5$ per group).

with immune checkpoint therapeutics and chemotherapies in cancer patients. In this study, we developed an immuno-PET technique that can non-invasively image CD73 status in tumors of living mice.

The rat IgG2a (TY/23) monoclonal antibody in this study reacts with the glycosylphosphatidylinositol-anchored cell-surface protein of mouse CD73 and has been used in several previous studies to detect CD73 and investigate its function^{14,22–24}. This antibody has a reported affinity against murine CD73 protein similar to another antibody with a K_d of 169 nM²⁵. The antibody was designed specific for mouse CD73 to detect and study its expression in murine samples, with no report of cross reactivity with CD73 from human or other species. The high target binding capacity of the anti-CD73 TY/23 clone was shown in CD73-expressing mouse 4T1 mammary carcinoma cells. The clone further elicited a stronger suppression of CT26 tumors over other monoclonal antibody clones²². The TY/23 antibody was shown to block tumor angiogenesis during in vivo anti-tumor therapy²³. The antibody also enhanced the antitumor activity of anti-PD-1 and anti-CTLA-4 antibodies in MC38-OVA and 4T1.2 tumors¹⁴.

In a recent study, Sudo et al. radiolabeled a human anti-CD73 monoclonal antibody (067-213) with ^{111}In . Subsequently, single-photon emission computed tomography imaging and biodistribution studies in a mouse model showed that tumor uptake of the ^{111}In -labeled antibody reflected CD73 expression levels¹⁸. However, PET imaging is required for greater spatial resolution and provision of quantitative information.

^{89}Zr has a 3.3-day physical half-life and allows delayed PET imaging that is required for intact antibodies with relatively long circulating times. Antibodies labeled with ^{89}Zr antibodies can be used for non-invasive PET imaging of target status in living bodies. Our group established a cysteine site-specific ^{89}Zr conjugation as an elegant way of tailoring the location of ^{89}Zr attachment to antibodies for immuno-PET imaging²⁰. In this study, cysteine site-specific ^{89}Zr conjugation of anti-CD73 TY/23 antibody was achieved in a straightforward fashion with a radiolabeling yield of approximately 80%. A short 1-h reaction at room temperature was sufficient, which contrasts with the ^{111}In radiolabeling procedure in the previous study that required a long reaction time at 37°C ¹⁸.

For our study purpose, we used low-expressing CT26 mouse colon cancer cells engineered to constitutively overexpress CD73 (CT26/CD73 cells) as well as 4T1.2 mouse breast cancer cells that express physiological

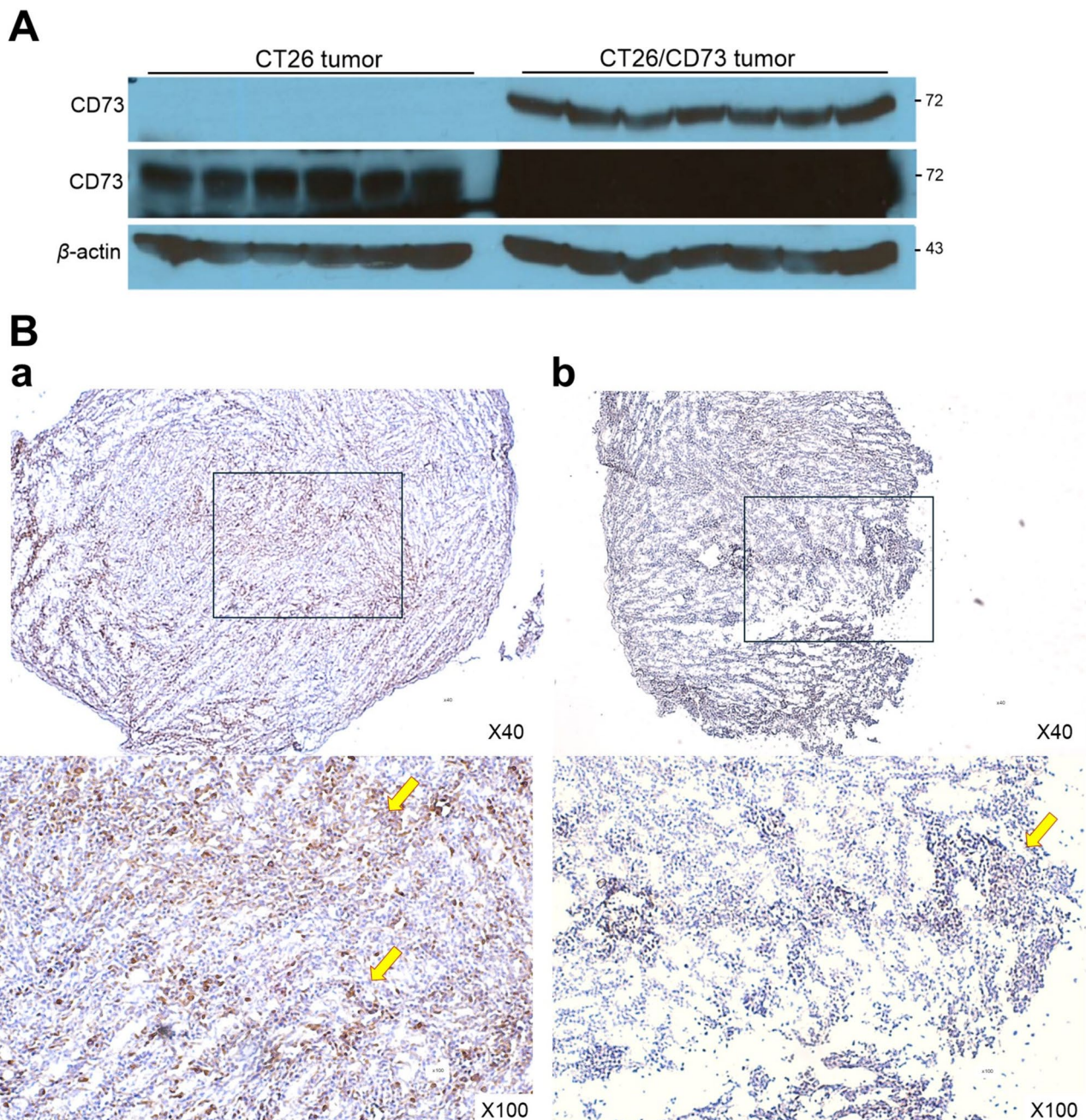


Figure 6. CD73 expression in CT26 and CT26/CD73 tumor tissues. (A) Immunoblotting for CD73 and β -actin. Note that CD73 bands in CT26 tumors were detected only by long exposure times (middle) while they were detected in CT26/CD73 tumors by short exposure times (top). (B) Immunohistochemistry showing strong CD73 staining in CT26/CD73 tumors (a) and weak staining in CT26 tumors (b). Arrows point to tumor cells with positive CD73 staining. The area in the box for the lower magnified images (top; $\times 40$) are shown in the higher magnified images (bottom $\times 100$).

(moderate) levels of CD73. Cell binding assays revealed substantially greater ^{89}Zr -CD73 IgG binding in both cells compared to parental CT26 cells. Excellent target specificity of the binding was confirmed by complete suppression of uptake by competitive inhibition with excess unlabeled CD73 IgG. Furthermore, the ^{89}Zr -CD73 IgG uptake level showed near-perfect linear correlation to the amounts of CT26/CD73 cells mixed with graded portions of low-expressing CT26 cells, indicating that target amount was faithfully reflected by ^{89}Zr -CD73 IgG uptake level in vitro.

When injected into mouse models, ^{89}Zr -CD73 IgG PET visualized CT26/CD73 tumors as well as 4T1.2 tumors with high tumor-to-background uptake by 8 days post-injection, whereas CT26 tumors showed low uptake contrast. The biodistribution results verified that ^{89}Zr -CD73 IgG uptake was high in CT26/CD73 tumors and 4T1.2 tumors but low in parental CT26 tumors. Although CT26/CD73 and 4T1.2 tumor activities appeared similar

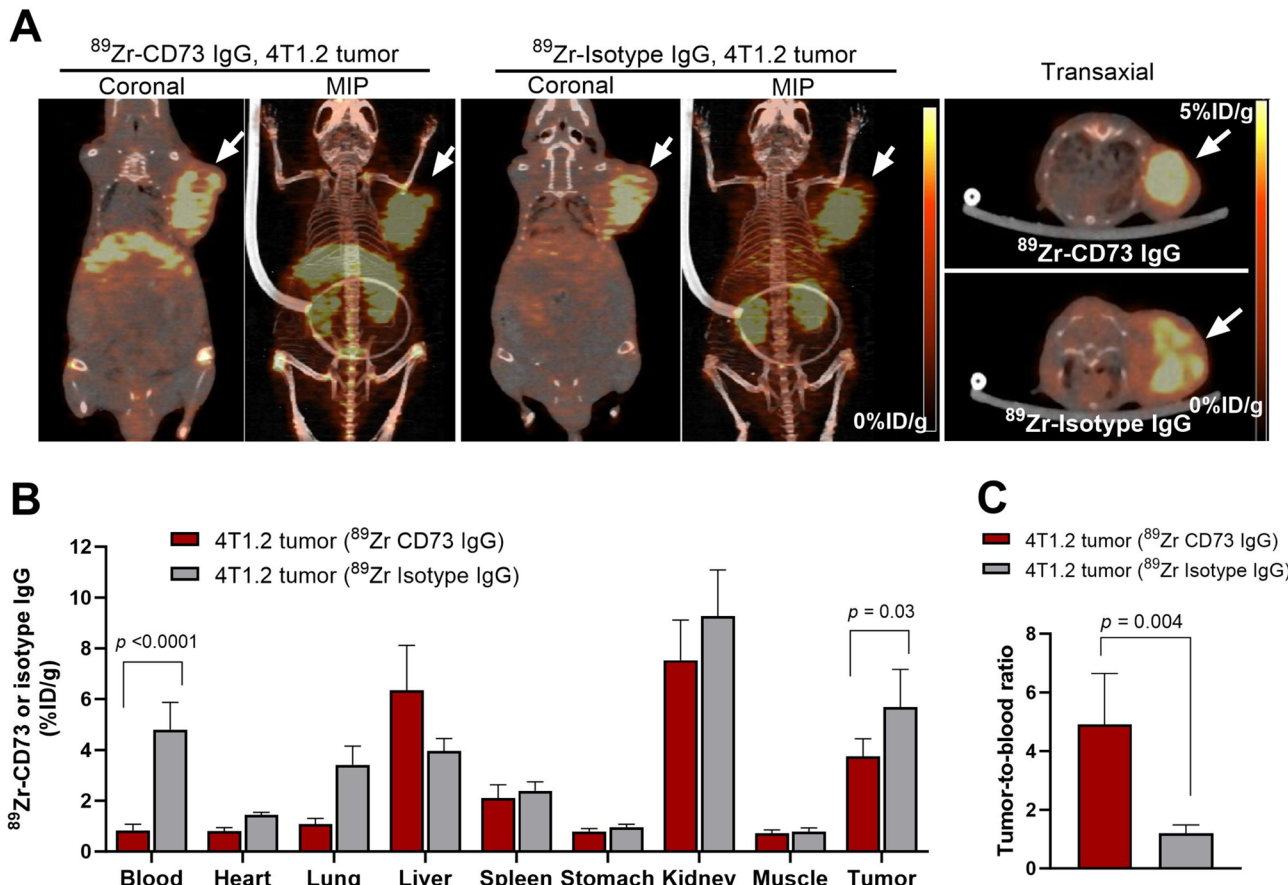


Figure 7. ⁸⁹Zr-CD73 IgG PET/CT and biodistribution at 8 days in 4T1.2 tumor mice. (A) Coronal tomographic and maximum intensity-projection (MIP) ⁸⁹Zr-CD73 (left) and ⁸⁹Zr-isotype IgG (middle) PET/CT in mice bearing CT26/CD73 tumors. Transaxial tomographs are shown in the right. (B) Biodistribution data of mice as above at 8 days post-injection. (C) Again, the CT26/CD73 tumor-to-blood ratio was significantly higher for ⁸⁹Zr-CD73 IgG compared to ⁸⁹Zr-isotype IgG. Data are presented as the mean \pm standard error of obtained from two independent experiments ($n=5$ per group).

for ⁸⁹Zr-CD73 IgG and control ⁸⁹Zr-isotype IgG, the slow blood clearance of the latter compared to the relatively rapid clearance of the former is of crucial importance in understanding the specificity of the tumor activities. Indeed, the low tumor-to-blood ratio compared to the high ratios for ⁸⁹Zr-CD73 IgG in CT26/CD73 and 4T1.2 tumors indicate that the tumor activity of ⁸⁹Zr-isotype IgG was likely largely contributed by high intra-tumoral blood activity of the antibody that was poorly extracted from the circulation from lack of binding target. Other previous studies have evidenced target-specific tumor uptake of ⁸⁹Zr-labeled specific IgG using an ⁸⁹Zr-isotype IgG that showed similar tumor activity but with high blood pool activity. Interestingly, this includes a study that used an ⁸⁹Zr-labeled in vivo grade isotype rat IgG2 from BioXcell²⁶, similar to the in vivo grade isotype IgG2 that was used in the present study. This isotype antibody is considered the most accurate control for the BioXcell's anti-CD73 antibody, and other investigators have used the same set of anti-CD73 (clone TY/23) and rat isotype control antibody (clone 2A3) for in vivo experiments^{27,28}.

In comparison, the rapid blood clearance of ⁸⁹Zr-CD73 IgG was likely contributed by prompt recognition and binding to CD73 targets on tumor cells and CD73-expressing normal cells/tissues, which resulted in their swift extraction from the blood. Although not as high as in tumors, CD73 is ubiquitously expressed in multiple organs and certain normal cells, where it regulates tissue homeostasis²⁹. This includes normal kidney cells, lung epithelial cells, liver cells, and endothelial cells^{30–32}. Among immune cells, CD73 is expressed on a portion of CD4+ and CD8+ T cells and is broadly expressed in peripheral blood B cells. Tissue macrophages and neutrophils can also express CD73, whereas it is virtually absent in NK cells³³. We used Balb/c nude mice that lack mature T-cells, but binding to B cells and macrophages could have partly contributed to blood clearance of the antibody. As such, CD73 expression in the tumor and in certain normal organs/cells of the host mice likely influenced the biodistribution of ⁸⁹Zr-CD73 IgG and appears to have facilitated its clearance from the circulation. Contribution from antibody aggregation or dissociation into half-molecules (which occurs mostly with IgG4) was not likely a major factor, since it would have lowered tumor uptake due to rapid liver accumulation and renal excretion, respectively.

As for the ⁸⁹Zr-CD73 IgG uptake in CT26 tumors, a significant portion was likely specific targeting of weakly expressed CD73, while a portion may have been due to passive non-specific accumulation by enhanced

permeability and retention (EPR). The EPR effect may also explain part of the nonspecific ^{89}Zr -Isotype IgG uptake in CT26/CD73 tumors.

The previous ^{111}In -067-213 antibody study showed high blood uptake at 4 days post-injection that exceeded 10%ID/g in two tumor models¹⁸. In comparison, our results showed low blood activity of ^{89}Zr -CD73 IgG at 4 days. However, there was relatively high ^{89}Zr -CD73 IgG remaining in the kidneys, liver, and spleen at this early time point, indicating that a more delayed imaging time would be more optimal for evaluating intraabdominal tumors. This was confirmed by an additional group of mice studied at a later time point of 8 days post-injection that showed similar uptake in the tumors but lowered activities in normal organs.

A limitation of our study is that murine cancer cells were used for experiments without the inclusion of human origin cancer cells, which could constrain the potential of ^{89}Zr -CD73 IgG for future translation.

CD73 inhibitors are considered promising as single agents or in combination with other immune checkpoint blockers for advanced cancer immunotherapy^{13,14,34}. Therefore, noninvasive assessment of tumor CD73 status with ^{89}Zr -CD73 IgG PET could be useful for screening cancer patients who are likely to benefit from CD73-inhibiting drugs for improved immunotherapy response.

Conclusions

^{89}Zr -CD73 IgG showed CD73-dependent specific binding to cancer cells, displaying favorable in vivo biodistribution, and provided high contrast PET imaging of CD73 expressing tumors. Thus, ^{89}Zr -CD73 IgG PET may be useful for the non-invasive assessment of tumor CD73 expression in living subjects.

Data availability

All data generated or analyzed during this study are included in this published article [and its supplementary information files].

Received: 15 November 2023; Accepted: 30 July 2024

Published online: 03 August 2024

References

1. de Leve, S., Wirsdörfer, F. & Jendrossek, V. The CD73/Ado system—A new player in RT induced adverse late effects. *Cancers* **11**(10), 1578. <https://doi.org/10.3390/cancers11101578> (2019).
2. Chen, S. *et al.* CD73 expression on effector T cells sustained by TGF- β facilitates tumor resistance to anti-4-1BB/CD137 therapy. *Nat. Commun.* **10**(1), 150. <https://doi.org/10.1038/s41467-018-08123-8> (2019).
3. Zhou, Y. *et al.* High expression of CD73 contributes to poor prognosis of clear-cell renal cell carcinoma by promoting cell proliferation and migration. *Transl. Cancer Res.* **11**(10), 3634–3644. <https://doi.org/10.21037/tcr-22-544> (2022).
4. Petruk, N. *et al.* CD73 facilitates EMT progression and promotes lung metastases in triple-negative breast cancer. *Sci. Rep.* **11**(1), 6035. <https://doi.org/10.1038/s41598-021-85379-z> (2021).
5. Nicole, M., Anderson, M. & Simon, C. Tumor microenvironment. *Curr. Biol.* **30**(16), R921–R925. <https://doi.org/10.1016/j.cub.2020.06.081> (2020).
6. Vijayan, D., Young, A., Teng, M. W. L. & Smyth, M. J. Targeting immunosuppressive adenosine in cancer. *Nat. Rev. Cancer* **17**(12), 709–724. <https://doi.org/10.1038/nrc.2017.110> (2017).
7. Chen, S. *et al.* CD73: An emerging checkpoint for cancer immunotherapy. *Immunotherapy* **11**(11), 983–997. <https://doi.org/10.2217/imt-2018-0200> (2019) (epub 2019 Jun 21).
8. Li, X. Y. *et al.* Targeting CD39 in cancer reveals an extracellular ATP- and inflammasome-driven tumor immunity. *Cancer Discov.* **9**(12), 1754–1773. <https://doi.org/10.1158/2159-8290.CD-19-0541> (2019).
9. Sek, K. *et al.* Targeting adenosine receptor signaling in cancer immunotherapy. *Int. J. Mol. Sci.* **19**(12), 3837. <https://doi.org/10.3390/ijms19123837> (2018).
10. Sharma, P. *et al.* Immune checkpoint therapy—Current perspectives and future directions. *Cell* **186**(8), 1652–1669. <https://doi.org/10.1016/j.cell.2023.03.006> (2023).
11. Topalian, S. L. *et al.* Safety, activity, and immune correlates of anti-PD-1 antibody in cancer. *N. Engl. J. Med.* **366**(26), 2443–2454. <https://doi.org/10.1056/NEJMoa1200690> (2012).
12. Tumeh, P. C. *et al.* PD-1 blockade induces responses by inhibiting adaptive immune resistance. *Nature* **515**(7528), 568–571. <https://doi.org/10.1038/nature13954> (2014).
13. Kurago, Z. *et al.* Inhibitors of the CD73-adenosinergic checkpoint as promising combinatory agents for conventional and advanced cancer immunotherapy. *Front. Immunol.* **14**, 1212209. <https://doi.org/10.3389/fimmu.2023.1212209> (2023).
14. Allard, B., Pommey, S., Smyth, M. J. & Stagg, J. Targeting CD73 enhances the antitumor activity of anti-PD-1 and anti-CTLA-4 mAbs. *Clin. Cancer Res.* **19**(20), 5626–5635. <https://doi.org/10.1158/1078-0432.CCR-13-0545> (2013).
15. Hay, C. M. *et al.* Targeting CD73 in the tumor microenvironment with MEDI9447. *Oncoimmunology* **5**(8), e1208875. <https://doi.org/10.1080/2162402X.2016.1208875> (2016).
16. Ehlerding, E. B., England, C. G., McNeil, D. G. & Cai, W. Molecular imaging of immunotherapy targets in cancer. *J. Nucl. Med.* **57**(10), 1487–1492. <https://doi.org/10.2967/jnumed.116.177493> (2016).
17. Brodská, B. *et al.* High PD-L1 expression predicts for worse outcome of leukemia patients with concomitant NPM1 and FLT3 mutations. *Int. J. Mol. Sci.* **20**(11), 2823. <https://doi.org/10.3390/ijms20112823> (2019).
18. Sudo, H. *et al.* Radiolabeled human monoclonal antibody 067-213 has the potential for noninvasive quantification of CD73 expression. *Int. J. Mol. Sci.* **21**(7), 2304. <https://doi.org/10.3390/ijms21072304> (2020).
19. Lee, K.-H., Jung, K.-H. & Lee, J. H. Immuno-PET imaging and radioimmunotherapy of lymphomas. *Mol. Pharm.* **19**(10), 3484–3491. <https://doi.org/10.1021/acs.molpharmaceut.2c00563> (2022).
20. Jung, K.-H. *et al.* ^{89}Zr -labeled anti-PD-L1 antibody PET monitors gemcitabine therapy-induced modulation of tumor PD-L1 expression. *J. Nucl. Med.* **62**(5), 656–664. <https://doi.org/10.2967/jnumed.120.250720> (2021).
21. Lindmo, T., Boven, E., Cuttitta, F., Fedorko, J. & Bunn, P. A. Jr. Determination of the immunoreactive fraction of radiolabeled monoclonal antibodies by linear extrapolation to binding at infinite antigen excess. *J. Immunol. Methods* **72**(1), 77–89. [https://doi.org/10.1016/0022-1759\(84\)90435-6](https://doi.org/10.1016/0022-1759(84)90435-6) (1984).
22. Vijayana, D. *et al.* Selective activation of anti-CD73 mechanisms in control of primary tumors and metastases. *Oncoimmunology* **6**(5), e1312044. <https://doi.org/10.1080/2162402X.2017.1312044> (2017).
23. Allard, B. *et al.* Anti-CD73 therapy impairs tumor angiogenesis. *Int. J. Cancer* **134**, 1466–1473. <https://doi.org/10.1002/ijc.28456> (2014).

24. Zhang, F. *et al.* Specific decrease in B-cell-derived extracellular vesicles enhances post-chemotherapeutic CD8+ T cell responses. *Immunity* **50**(3), 738–750. <https://doi.org/10.1016/j.immuni.2019.01.010> (2019).
25. Vijayan, D. *et al.* Selective activation of anti-CD73 mechanisms in control of primary tumors and metastases. *Oncoimmunology* **6**(5), e1312044 (2017).
26. Beckford Vera, D. R. *et al.* Immuno-PET imaging of tumor-infiltrating lymphocytes using zirconium-89 radiolabeled anti-CD3 antibody in immune-competent mice bearing syngeneic tumors. *PLoS ONE* **13**(3), e0193832 (2023).
27. Yu, M. *et al.* CD73 on cancer-associated fibroblasts enhanced by the A2B-mediated feedforward circuit enforces an immune checkpoint. *Nat. Commun.* **11**, 515 (2020).
28. Tsukui, H. *et al.* CD73 blockade enhances the local and abscopal effects of radiotherapy in a murine rectal cancer model. *BMC Cancer* **20**, 411 (2020).
29. Yan, H. *et al.* CD73, tumor plasticity and immune evasion in solid cancers. *Cancers* **13**, 177 (2021).
30. Roh, M. *et al.* Targeting CD73 to augment cancer immunotherapy. *Curr. Opin. Pharmacol.* **53**, 66–76 (2020).
31. Sciarra, A. *et al.* CD73 expression in normal and pathological human hepatobiliarypancreatic tissues. *Cancer Immunol. Immunother.* **68**(3), 467–478 (2019).
32. Alcedo, K. P. *et al.* CD73 maintains hepatocyte metabolic integrity and mouse liver homeostasis in a sex-dependent manner. *Cell Mol. Gastroenterol. Hepatol.* **12**(1), 141–157 (2021).
33. Allard, B., Longhi, M. S., Robson, S. C. & Stagg, J. The ectonucleotidases CD39 and CD73: Novel checkpoint inhibitor targets. *Immunol. Rev.* **276**(1), 121–144 (2017).
34. Tahkola, K. *et al.* Prognostic impact of CD73 expression and its relationship to PD-L1 in patients with radically treated pancreatic cancer. *Virchows Arch.* **478**(2), 209–217. <https://doi.org/10.1007/s00428-020-02888-4> (2021).

Acknowledgements

This research was supported by the Basic Science Research Program through the National Research Foundation of Korea (NRF) grant funded by the Korean government (MIST) (2022R1A2B5B01001216 & RS-2024-00337150).

Author contributions

K.-H.J. co-wrote the original manuscript text and funding acquisition. M.K., H.J.J, H.J.K., J.L.K., and H.L. prepared figures. K.-H.L., co-wrote the original manuscript text and supervised the Project.

Competing interests

The authors declare no competing interests.

Additional information

Supplementary Information The online version contains supplementary material available at <https://doi.org/10.1038/s41598-024-68987-3>.

Correspondence and requests for materials should be addressed to K.-H.L.

Reprints and permissions information is available at www.nature.com/reprints.

Publisher's note Springer Nature remains neutral with regard to jurisdictional claims in published maps and institutional affiliations.

Open Access This article is licensed under a Creative Commons Attribution-NonCommercial-NoDerivatives 4.0 International License, which permits any non-commercial use, sharing, distribution and reproduction in any medium or format, as long as you give appropriate credit to the original author(s) and the source, provide a link to the Creative Commons licence, and indicate if you modified the licensed material. You do not have permission under this licence to share adapted material derived from this article or parts of it. The images or other third party material in this article are included in the article's Creative Commons licence, unless indicated otherwise in a credit line to the material. If material is not included in the article's Creative Commons licence and your intended use is not permitted by statutory regulation or exceeds the permitted use, you will need to obtain permission directly from the copyright holder. To view a copy of this licence, visit <http://creativecommons.org/licenses/by-nc-nd/4.0/>.

© The Author(s) 2024